

Supplementary material

Text S1. Historical land-use data provided by ISIMIP2a

In the historical land-use data provided by ISIMIP2a, the cropland and pasture area in 2000 was derived from Ramankutty et al., (2008). Total cropland and pasture area was then extrapolated into the past and future using trends from HYDE3 (Klein Goldewijk et al., 2011), while the MIRCA2000 crop dataset (Portmann et al., 2010) was further used to differentiate major crop types, and rainfed and irrigated parts (see appendix of Fader et al., 2010 for detail of the land-use dataset).

Text S2. The net land carbon fluxes derived from the Global Carbon Project (GCP) carbon budget

The GCP carbon budget reported by Le Quéré et al., (2015) provided an estimate of the land carbon balance decomposed into two components: net land-use change emissions (E_{LUC}) and the ‘residual’ land sink (RLS). E_{LUC} was calculated based on the national forest area loss statistics published by the United Nations Food and Agriculture Organization and a bookkeeping model (Houghton et al., 2012) to convert forest area changes into net CO₂ fluxes, including legacy regrowth of past cohorts of deforested areas and soil CO₂ emissions or accumulation after land-use change. E_{LUC} was also compared, and found to be consistent on a decadal basis, with the ‘land use flux’ simulated with the TRENDY models from the difference between a simulation with and one without land cover change (see Pongratz et al. 2014 and Gasser and Ciais, 2013 for differences between different approaches to calculate E_{LUC}). The RLS was by construction “the difference between, on the one hand, fossil fuel and land-use-change emissions and, on the other hand, the growth rate in atmospheric CO₂ concentration and the ocean CO₂ sink” (Le Quéré et al., 2015).

Text S3. ENSO events defined by Multivariate ENSO Index (MEI)

Evaluation of modeled carbon flux anomalies in ENSO events requires a proper definition of ENSO events. In this study, ENSO events were defined by the MEI index. MEI was based on six observed variables over the tropical Pacific (Wolter and Timlin, 2011). The value of MEI time series and historic bimonthly ranks were accessed in March, 2016 from <http://www.esrl.noaa.gov/psd/enso/mei/>, where historic

events since 1950 are available. We used the quintile definition for ‘moderate or strong’ ENSO events, where MEI bimonthly ranks from 1-13 denote La Niña, while those with ranks of 54-66 (or 55-67 depending on available number of bimonthly MEI) denote El Niño. Years with at least three bimonthly rankings in the top ranks (1-13 for La Niña and 54-66 for El Niño) were considered as La Niña or El Niño years, respectively. For the model evaluation period (since 1971), 11 La Niña years (1971, 1973, 1974, 1975, 1976, 1988, 1989, 1999, 2000, 2008, 2010) and 13 El Niño years (1972, 1982, 1983, 1987, 1991, 1992, 1993, 1994, 1995, 1997, 1998, 2002, 2009) were considered.

Text S4. Normalized difference vegetation index (NDVI) data

Normalized difference vegetation index (NDVI) was used as a proxy to measure vegetation greenness. It has been proven to be positively correlated with terrestrial ecosystems productivity (Myneni et al 1997, Bunn and Goetz, 2006). In this study, we used the NOAA/AVHRR composite NDVI at a spatial resolution of 8-km and 15-day intervals produced by the Global Inventory Modeling and Mapping Studies (GIMMS; Tucker et al., 2005) from 1982 onwards. To reduce the noise (e.g. from variable cloud cover), we used monthly NDVI from two values for each month based on the maximum value composite (MVC) method (Holben, 1986). Monthly NDVI data was aggregated to annual value and to the spatial resolution of $0.5^{\circ} \times 0.5^{\circ}$, and used in this study as a proxy for observed above-ground ecosystem productivity. We focused on carbon fluxes over vegetated land, defined as the land grid cells with mean NDVI larger than 0.1 over the period 1982-2010.

Text S5. Land-atmosphere CO₂ fluxes from atmospheric inversion systems

Atmospheric inversion systems provide surface CO₂ fluxes including fossil and land-use-change emissions and land and ocean CO₂ fluxes, based on a worldwide network of atmospheric measurements and atmospheric inversion methods. The total land fluxes (combination of land-use-change emissions and land CO₂ fluxes) are suitable to be used to benchmark the NBP simulations from ISIMIP2a models. In this study, total land fluxes from two inversion systems were used for the same period of 1981-2010: the Jena CarboScope s81_v3.8 (original data available from 1981 to 2015; Rödenbeck et al., 2003; 2006; hereafter referred to as F_{Jena}), and CAMS v15r2

(original data available from 1979 to 2015; Chevallier et al., 2005, 2010; Chevallier, 2013; hereafter referred to as F_{CAM5}).

Reference:

Ramankutty, N., A. T. Evan, C. Monfreda and J. A. Foley (2008). "Farming the planet: 1. Geographic distribution of global agricultural lands in the year 2000." *Global Biogeochemical Cycles* 22(1).

Klein Goldewijk, K., A. Beusen, G. Van Drecht and M. De Vos (2011). "The HYDE 3.1 spatially explicit database of human- induced global land- use change over the past 12,000 years." *Global Ecology and Biogeography* 20(1): 73-86.

Portmann, F. T., S. Siebert and P. Döll (2010). "MIRCA2000—Global monthly irrigated and rainfed crop areas around the year 2000: A new high- resolution data set for agricultural and hydrological modeling." *Global Biogeochemical Cycles* 24(1).

Fader, M., S. Rost, C. Müller, A. Bondeau and D. Gerten (2010). "Virtual water content of temperate cereals and maize: Present and potential future patterns." *Journal of Hydrology* 384(3): 218-231.

Houghton, R. A., J. House, J. Pongratz, G. Van der Werf, R. DeFries, M. Hansen, C. L. Quéré and N. Ramankutty (2012). "Carbon emissions from land use and land-cover change." *Biogeosciences* 9(12): 5125-5142.

Le Quéré, C., R. Moriarty, R. M. Andrew, J. G. Canadell, S. Sitch, J. I. Korsbakken, P. Friedlingstein, G. P. Peters, R. J. Andres and T. Boden (2015). "Global carbon budget 2015." *Earth System Science Data* 7(2): 349-396.

Pongratz, J., C. H. Reick, R. Houghton and J. House (2014). "Terminology as a key uncertainty in net land use and land cover change carbon flux estimates." *Earth System Dynamics* 5(1): 177.

Gasser, T. and P. Ciais (2013). "A theoretical framework for the net land-to-atmosphere CO₂ flux and its implications in the definition of" emissions from

- land-use change". *Earth System Dynamics* 4(1): 171-186.
- Wolter, K. and M. S. Timlin (2011). "El Niño/Southern Oscillation behaviour since 1871 as diagnosed in an extended multivariate ENSO index (MEI. ext)." *International Journal of Climatology* 31(7): 1074-1087.
- Myneni, R.B., C.D. Keeling, , C.J. Tucker, G. Asrar, and R.R, Nemani (1997). "Increased plant growth in the northern high latitudes from 1981 to 1991. " *Nature*, 386: 698–702.
- Holben, B. N. (1986). "Characteristics of maximum-value composite images from temporal AVHRR data." *International journal of remote sensing* 7(11): 1417-1434.
- Bunn, A. G. and S. J. Goetz (2006). "Trends in satellite-observed circumpolar photosynthetic activity from 1982 to 2003: the influence of seasonality, cover type, and vegetation density." *Earth Interactions* 10(12): 1-19.
- Tucker, C. J., J. E. Pinzon, M. E. Brown, D. A. Slayback, E. W. Pak, R. Mahoney, E. F. Vermote and N. El Saleous (2005). "An extended AVHRR 8- km NDVI dataset compatible with MODIS and SPOT vegetation NDVI data." *International Journal of Remote Sensing* 26(20): 4485-4498.
- Rödenbeck, C., T. Conway and R. Langenfelds (2006). "The effect of systematic measurement errors on atmospheric CO₂ inversions: a quantitative assessment." *Atmospheric Chemistry and Physics* 6(1): 149-161.
- Rödenbeck, C., S. Houweling, M. Gloor and M. Heimann (2003). "CO₂ flux history 1982–2001 inferred from atmospheric data using a global inversion of atmospheric transport." *Atmospheric Chemistry and Physics* 3(6): 1919-1964.
- Chevallier, F. (2013). "On the parallelization of atmospheric inversions of CO₂ surface fluxes within a variational framework." *Geoscientific Model Development* 6(3): 783-790.
- Chevallier, F., P. Ciais, T. Conway, T. Aalto, B. Anderson, P. Bousquet, E. Brunke, L. Ciattaglia, Y. Esaki and M. Fröhlich (2010). "CO₂ surface fluxes at grid

point scale estimated from a global 21 year reanalysis of atmospheric measurements." *Journal of Geophysical Research: Atmospheres* 115(D21).

Chevallier, F., M. Fisher, P. Peylin, S. Serrar, P. Bousquet, F. M. Bréon, A. Chédin and P. Ciais (2005). "Inferring CO₂ sources and sinks from satellite observations: Method and application to TOVS data." *Journal of Geophysical Research: Atmospheres* 110(D24).

Table S1. The key model processes impacting NBP components.

Model	Fire	Prescribed vegetation	Dynamic vegetation	Deforestation	Harvest		
					Crops	Forest	Grassland
CARAIB	Yes	No	Forest and natural grassland	No	No	No	
DLEM	No	All prescribed	No	Biomass goes into litter, woody debris, and product pools, and atmosphere (burning)	Yes	No	No
JULES	No	Cropland and pasture	Forest, shrubs, and natural grassland	Biomass goes into litter pool, no burning	No	No	No
LPJ-GUESS	Yes	Cropland and pasture	Forest and natural grassland	Biomass goes into litter pool, no burning	No	No	No
LPJmL	Yes	Cropland and pasture	Forest and natural grassland	Biomass goes into litter pool, no burning	Yes	No	Yes
ORCHIDEE	No	All prescribed	No	Biomass goes into litter pool, no burning	Yes	No	No
VEGAS	Yes	Cropland	Forest and grassland	Biomass goes into litter and product pools, top soil carbon goes into fast-decomposing litter pool to represent erosion after deforestation, no burning	Yes	Yes	No
VISIT	Yes	Cropland	Forest and grassland	Biomass goes into litter pool, no burning	Yes	Yes	No

Table S2 Global annual mean NBP simulated by ORCHIDEE and VISIT driven by different climate forcings in different model-intercomparison projects. Data averaged for the period 1971-2010.

Project	Climate forcings	NBP (Pg C yr ⁻¹)	
		ORCHIDEE	VISIT
ISIMIP2a	PGFv2	0.93 ± 0.75	2.29 ± 1.11
ISIMIP2a	GSWP3	0.88 ± 0.82	2.56 ± 1.42
TRENDY	CRU-NCEP	1.43 ± 0.92	0.73 ± 1.10
MsTMIP	CRU-NCEP	0.99 ± 0.39	0.94 ± 0.83

Table S3. The regional decadal-mean NBP over grid cells with intensive land-use change in the past decades (i.e., grid cells with more than 2% net change, either increase or decrease, in agricultural fraction during 1971-2010). The values account for 14 simulations considering land-use change (i.e., excluding CARAIB). Unit: $\text{gC m}^{-2}\text{yr}^{-1}$.

Period	North America		South America		Sub-Saharan Africa		Southeast Asia	
	PGFv2	GSWP3	PGFv2	GSWP3	PGFv2	GSWP3	PGFv2	GSWP3
1971-1980	24 ± 4	24 ± 7	17 ± 21	22 ± 20	4 ± 6	4 ± 8	18 ± 26	15 ± 22
1981-1990	29 ± 6	27 ± 10	6 ± 21	8 ± 19	-9 ± 10	-7 ± 10	17 ± 37	17 ± 33
1991-2000	37 ± 10	35 ± 9	10 ± 15	6 ± 17	-4 ± 12	-3 ± 12	12 ± 36	4 ± 33
2001-2010	34 ± 12	33 ± 11	2 ± 15	5 ± 13	8 ± 11	0 ± 10	45 ± 40	48 ± 37

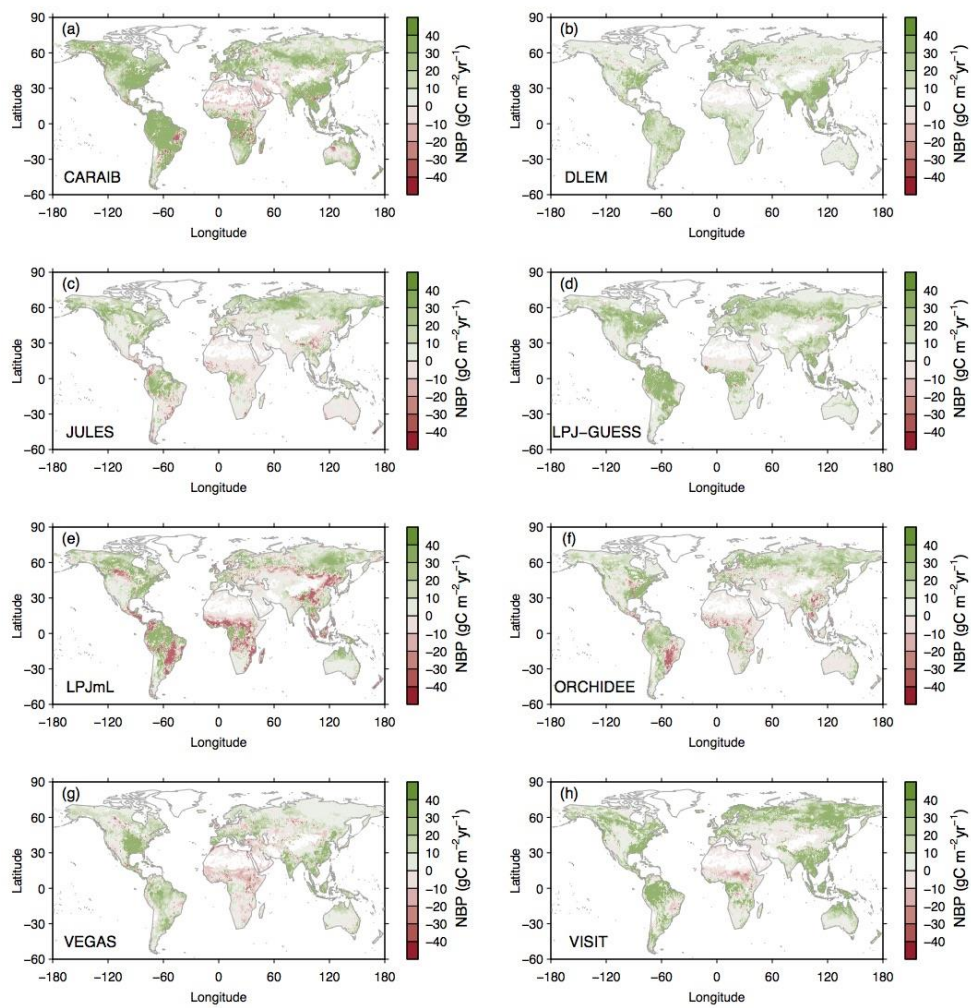


Figure S1. The spatial distribution of NBP simulated by eight ISIMIP2a biome models. The modeled NBP driven by the two climate forcing datasets is averaged for each model and for the period 1971-2010.

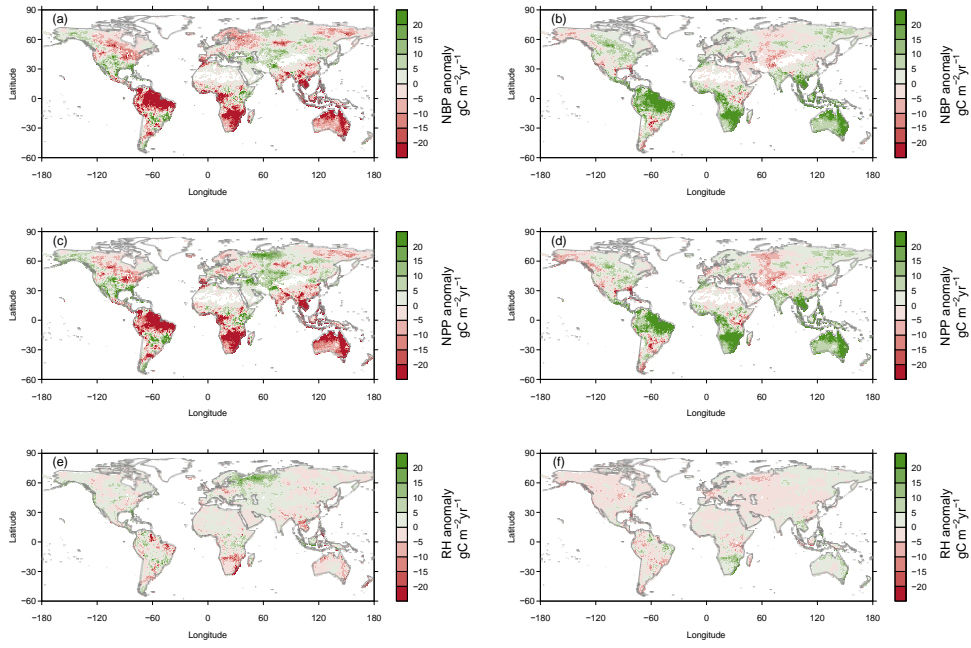


Figure S2. The spatial distribution of the ensemble-mean of (a-b) NBP anomaly, (c-d) NPP anomaly, and (e-f) Rh anomaly in years with significantly negative model ensemble-mean NBP anomaly (a, c, and e) and in years with significantly positive model ensemble-mean NBP anomaly (b, d, and f) respectively.

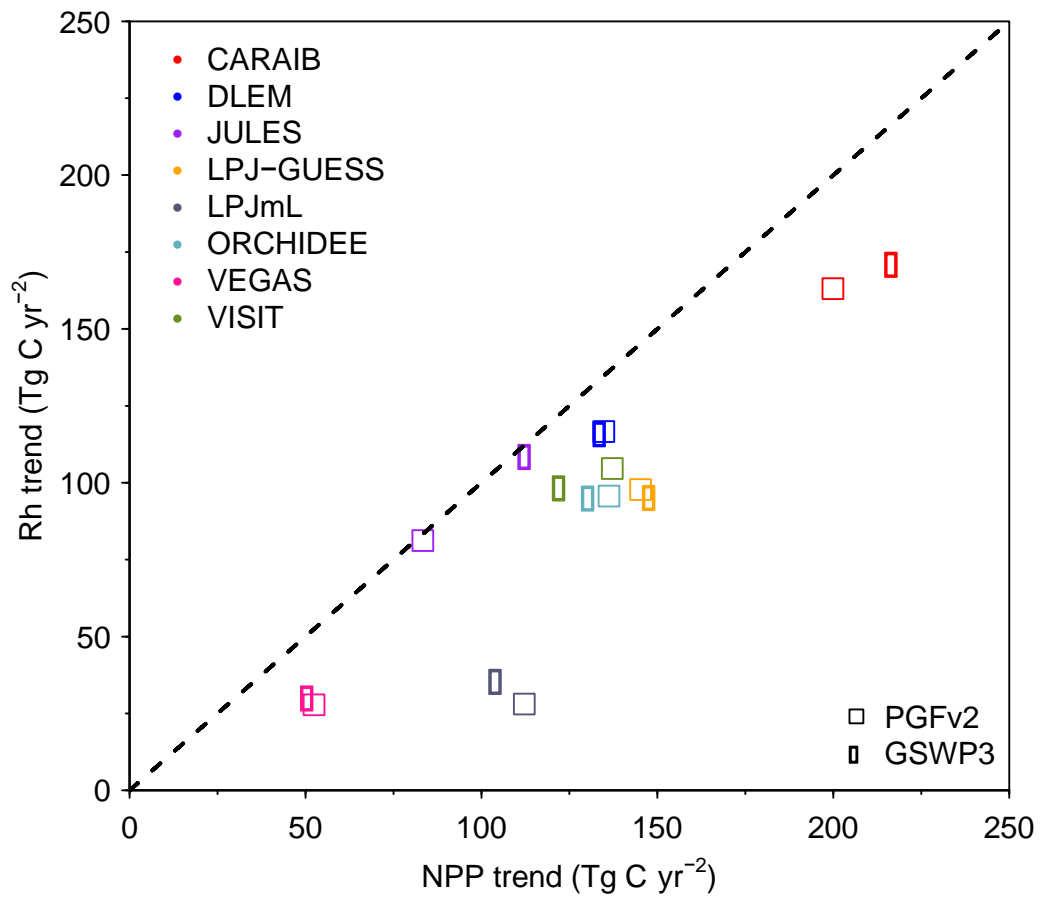


Figure S3. The trends of global NPP and Rh during 1971-2010 estimated by the eight ISIMIP2a biome models driven by the two climate forcing datasets respectively.

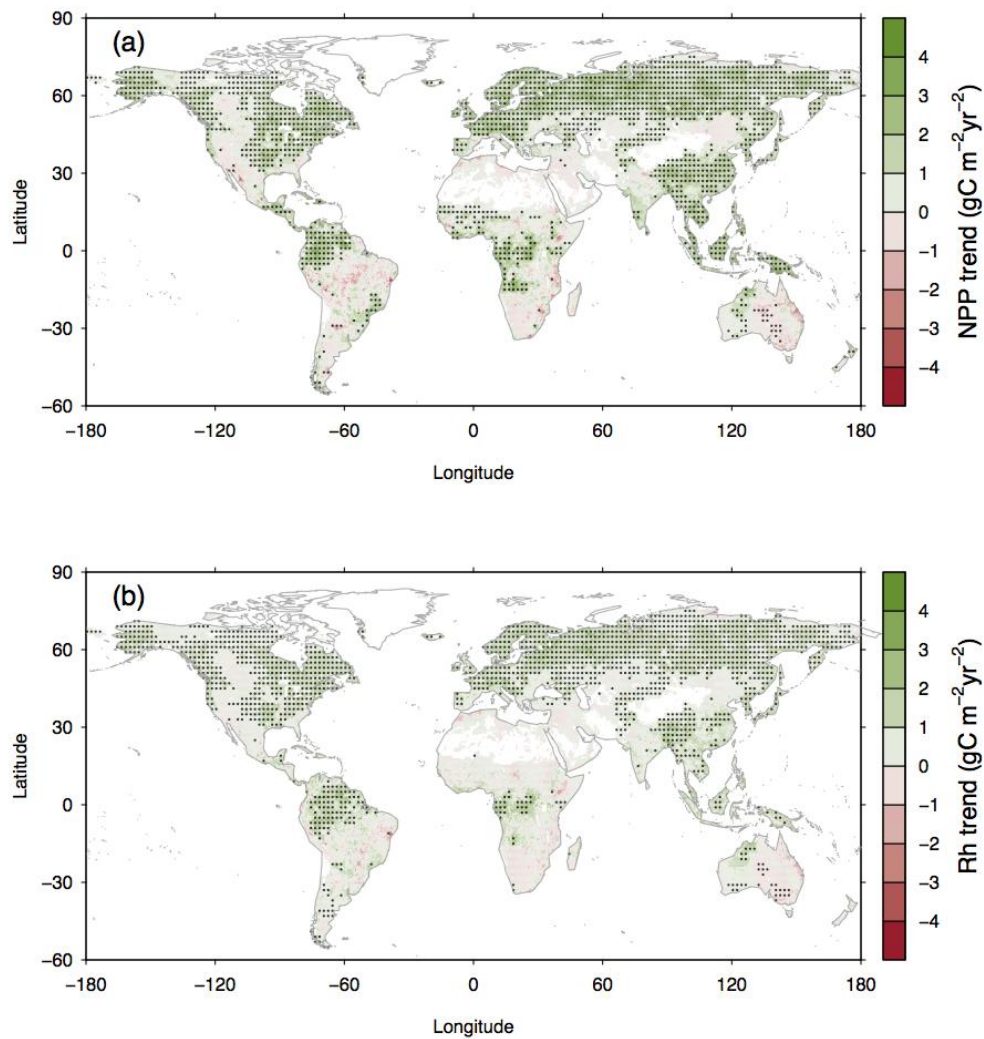


Figure S4. The spatial pattern of ensemble-mean (a) NPP trends and (b) Rh trends during the period 1971-2010. The stippled grid cells indicate the significant positive (or negative) NPP (or Rh) trends, and over 85% (i.e., 12 out of 14) of simulations considering land-use change (excluding CARAIB) agree on the sign of the trend. To present the stippled grid cells more clearly, each stipple is drawn at the resolution of $2^\circ \times 2^\circ$, where more than 8 out of 16 original grid cells ($0.5^\circ \times 0.5^\circ$ resolution) area stippled. The values over vegetated land (with annual mean NDVI larger than 0.1 over the period 1982-2010) are shown in the figure.

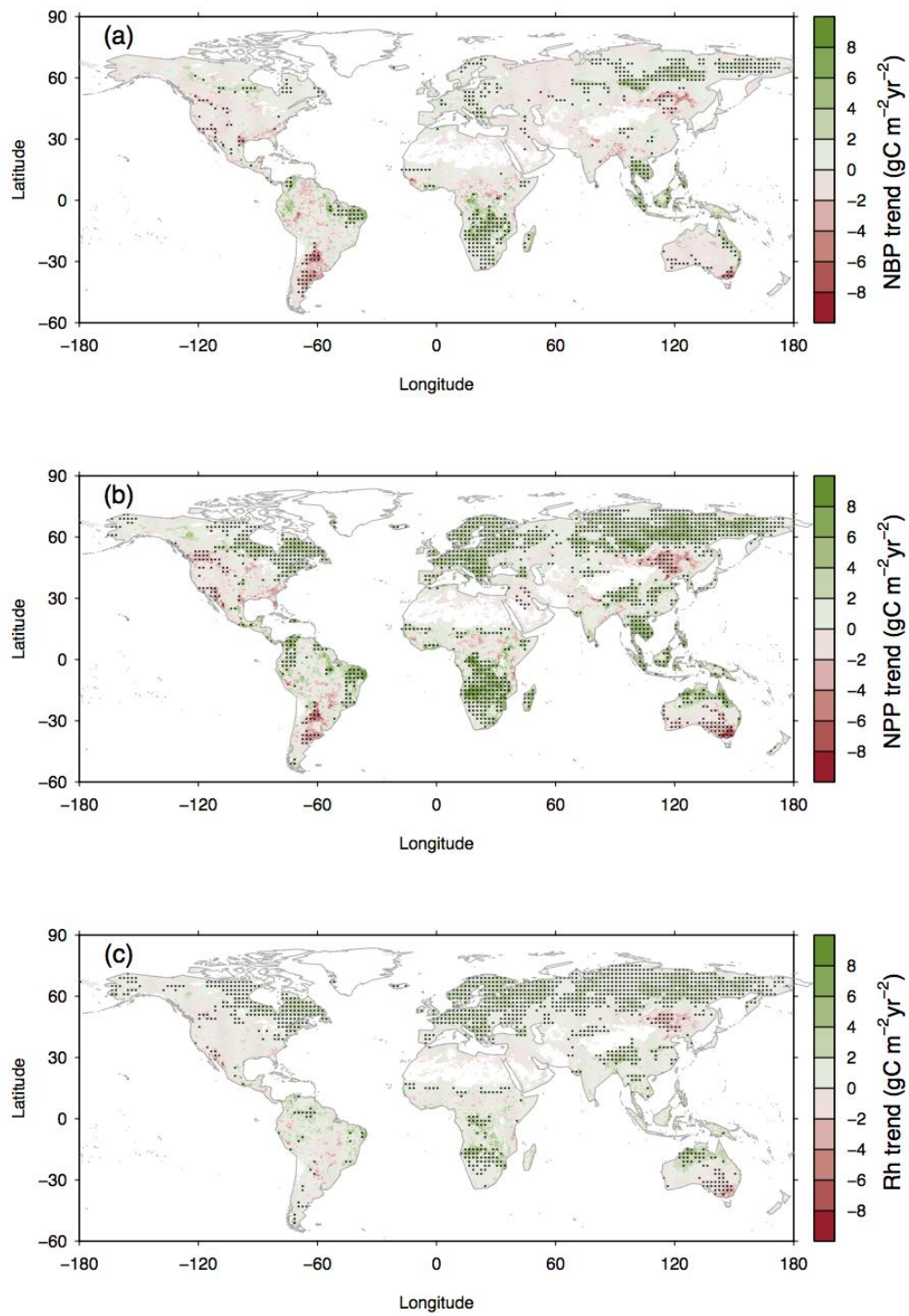


Figure S5. The spatial pattern of ensemble-mean of (a) NBP trends, (b) NPP trends and (b) Rh trends during the period 1990-2009. The stippled grid cells indicate the significant positive (or negative) NPP (or Rh) trends, and over 85% (i.e., 12 out of 14)

of simulations considering land-use change (excluding CARAIB) agree on the sign of the trend. To present the stippled grid cells more clearly, each stipple is drawn at a resolution of $2^\circ \times 2^\circ$, where more than 8 out of 16 original grid cells ($0.5^\circ \times 0.5^\circ$ resolution) area stippled. The values over vegetated land (with annual mean NDVI larger than 0.1 over the period 1982-2010) are shown in the figure.

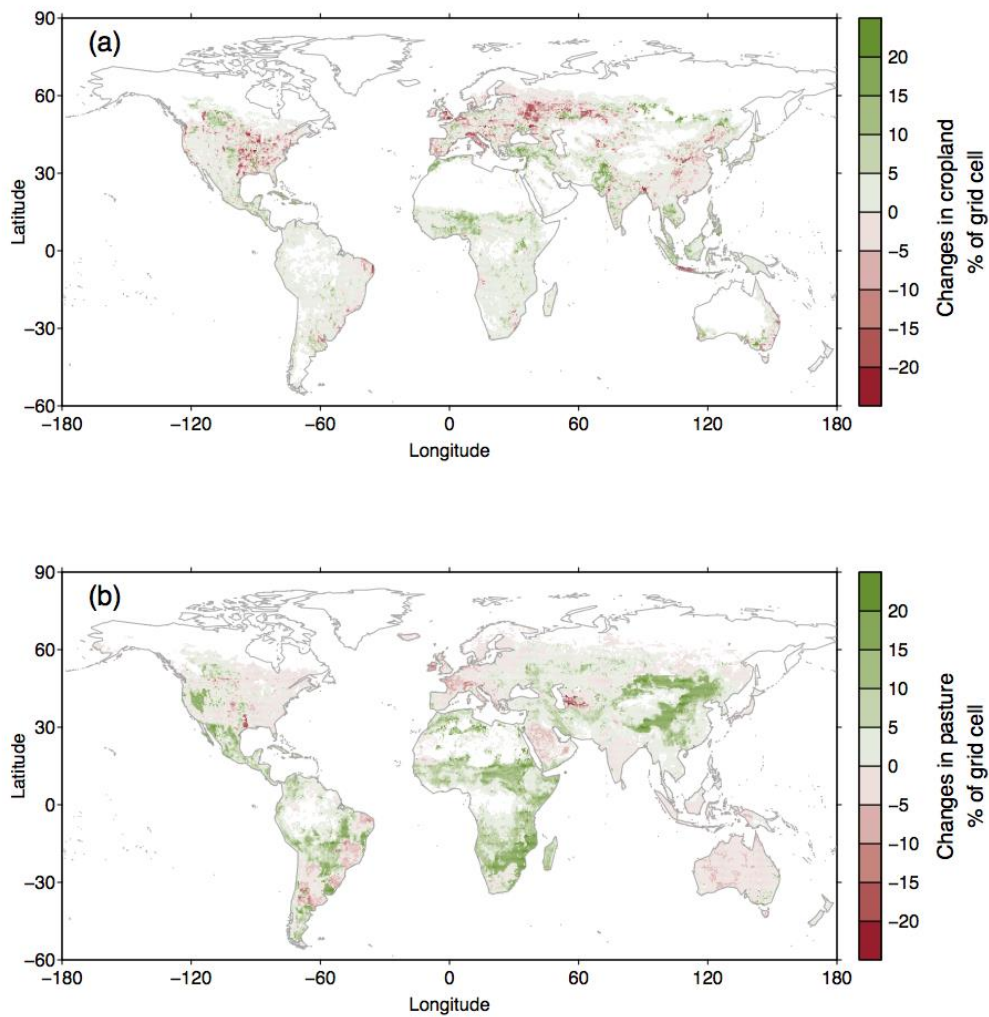


Figure S6. Changes in the fraction of (a) cropland and (b) pasture during 1971-2010. The changes are calculated by the difference of cropland/pasture fraction in each grid-cell between 2010 and 1971. Positive changes indicate increases in cropland/pasture area in the grid-cell, and vice versa. Data are derived from historical land-use data used as input to models (Ramankutty et al., 2008; Portmann et al., 2010; Klein Goldewijk et al., 2011).

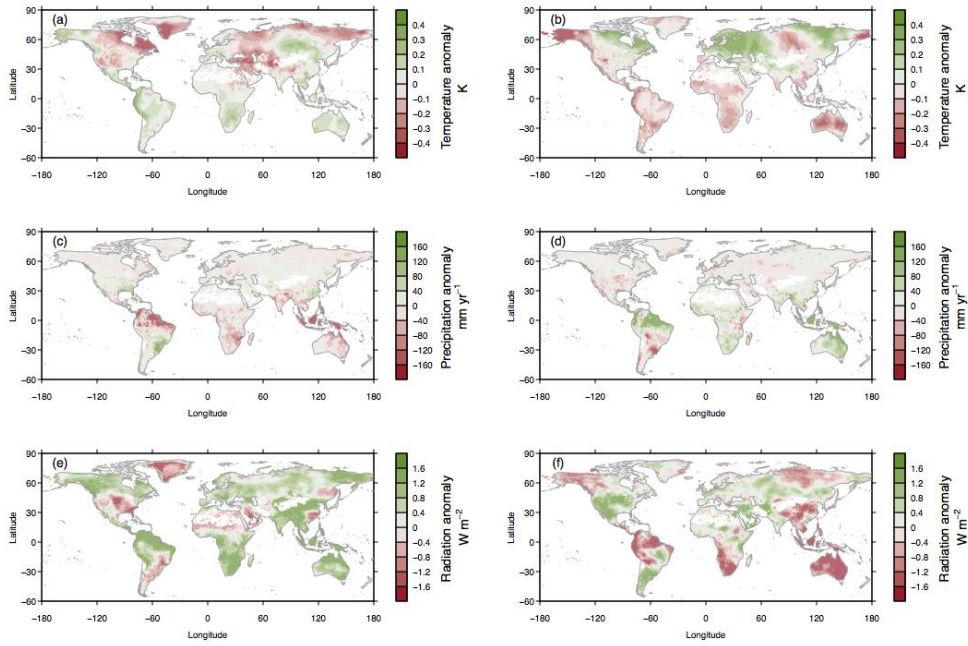


Figure S7. The spatial distribution of (a-b) temperature detrended anomaly, (c-d) precipitation detrended anomaly, and (e-f) solar radiation detrended anomaly in El Niño years (a, c, and e) and in La Niña years (b, d, and f) respectively. The detrended anomalies are averaged in El Niño / La Niña years from the two climate forcing datasets used in this study.